Monthly Notices
of the
ROYAL ASTRONOMICAL SOCIETY

Mon. Not. R. Astron. Soc. **404,** 2028–2036 (2010) doi:10.1111/j.1365-2966.2010.16418.x

SDSS J094533.99+100950.1 – the remarkable weak emission line quasar

K. Hryniewicz,[1,2]★ B. Czerny,[1] M. Nikołajuk[2] and J. Kuraszkiewicz[3]

[1]*Nicolaus Copernicus Astronomical Center, Bartycka 18, 00-716 Warsaw, Poland*
[2]*Faculty of Physics, University of Białystok, Lipowa 41, 15-424 Białystok, Poland*
[3]*Harvard-Smithsonian Center for Astrophysics, 60 Garden Street, Cambridge, MA 02138, USA*

Accepted 2010 January 25. Received 2010 January 25; in original form 2009 April 22

ABSTRACT

Weak emission line quasars are a rare and puzzling group of objects. In this paper, we present one more object of this class found in the Sloan Digital Sky Survey (SDSS). The quasar SDSS J094533.99+100950.1, lying at $z = 1.66$, has practically no C IV emission line, a red continuum very similar to the second steepest of the quasar composite spectra of Richards et al., is not strongly affected by absorption and the Mg II line, although relatively weak, is strong enough to measure the black hole mass. The Eddington ratio in this object is about 0.45, and the line properties are not consistent with the trends expected at high accretion rates. We propose that the most probable explanation of the line properties in this object, and perhaps in all weak emission line quasars, is that the quasar activity has just started. A disc wind is freshly launched so the low ionization lines which form close to the disc surface are already observed but the wind has not yet reached the regions where high ionization lines or narrow line components are formed. The relatively high occurrence of such a phenomenon may additionally indicate that the quasar active phase consists of several subphases, each starting with a fresh build-up of the broad-line region.

Key words: galaxies: active – quasars: absorption lines – quasars: emission lines – quasars: individual: SDSS J094533.99+100950.1.

1 INTRODUCTION

Strong, broad emission lines are the characteristic signature of active galactic nuclei (AGN). However, the Sloan Digital Sky Survey (SDSS) finds, among thousands of new AGN, rare objects with very weak or almost absent emission lines (Fan et al. 1999; Diamond-Stanic et al. 2009; Shemmer et al. 2009; Plotkin et al. 2010). Most of these objects, forming a new class of weak line quasars (hereafter referred to as WLQs), have been found primary at high redshifts ($z \gtrsim 2$). A few sources lying relatively close by have been studied in greater detail: PHL 1811 ($z = 0.19$; Leighly et al. 2007), PG 1407+265 ($z = 0.94$; McDowell et al. 1995) and HE 0141-3932 ($z = 1.80$; Reimers et al. 2005). The study of WLQs optical/ultraviolet (UV) continuum properties, X-ray and radio emission shows no obvious difference from typical emission line quasars and no apparent similarity to the weak-line BL Lac objects (Shemmer et al. 2009).

No generally accepted explanation for the weakness/absence of emission lines has been found so far. Possibilities so far considered include the following points. (1) Dust obscuration or extreme broad absorption line (BAL) effect, which is unlikely since there are no signs of the deep and broad absorption troughs in the spectra (Anderson et al. 2001; Collinge et al. 2005) and the X-ray absorbing column is low compared with BAL quasi-stellar objects (QSOs) ($N_{\rm H} < 5 \times 10^{22}$ cm^{-2}, Shemmer et al. 2009). (2) Gravitational lensing does not remove the emission lines (Shemmer et al. 2006), and strong C III] and C IV lines are found in gravitationally amplified quasars (e.g. Dobrzycki, Engels & Hagen 1999; Wayth, O'Dowd & Webster 2005). (3) Relativistic beaming is a good explanation for the absence of strong lines in BL Lac objects but WLQs, in contrast to BL Lacs, have bluer optical/UV continua, are radio quiet and show no variability or strong polarization (Diamond-Stanic et al. 2009; Shemmer et al. 2009). (4) The difference in the ionizing continuum also faces difficulties since at least the observed part of the continuum in those sources looks typical for a quasar. However, those objects may still emit more vigorously in the unobserved UV, thus having a higher accretion rate than the average quasars, which may affect the lines, as e.g. seen through the Baldwin effect. No black hole mass determination or Eddington ratio was possible for the sample of objects analysed by Shemmer et al. (2009) so as to confirm or reject this hypothesis. In this paper, we present a new WLQ object found in the SDSS survey which opens a possibility to address this issue.

2 SELECTION PROCEDURES AND OBSERVED PROPERTIES OF THE QUASAR SDSS J094533.99+100950.1

SDSS J094533.99+100950.1 was serendipitously discovered by us while searching the full SDSS Data Release 5 (SDSS DR5) (Adelman-McCarthy et al. 2007) spectral data base with the aim of

★E-mail: krhr@camk.edu.pl

finding interesting quasars for which atypical line and/or continuum properties would prohibit them being found and classified as quasars by the SDSS automatic pipeline. In particular, we looked for quasars with extreme blue continua (these would have been missed due to colour cuts used by the SDSS to avoid regions of colour space dominated by white dwarfs, A-stars and M star+white dwarf pairs – see Richards et al. 2002) and quasars with normal (unreddened by dust) continua but with non-standard emission line properties. We analysed all, 1 048 960, spectra available in the SDSS DR5 spectral data base, classified by the SDSS automatic procedures into galaxies, quasars, stars, sky and unclassifiable objects (see Adelman-McCarthy et al. 2007).

The spectrum of SDSS J094533.99+100950.1 appeared as particularly interesting, showing a normal quasar continuum but with atypical, weak emission lines, with practically non-existent C IV and C III] and weak, although clearly visible, Mg II. The object was identified as a quasar by the SDSS pipeline due to the presence of the Mg II line, and is hence also included in the Schneider et al. (2007) SDSS quasar catalogue. The spatial coordinates are $\alpha = 146.39163$, $\delta = 10.163927$ and the determined redshift is $z = 1.66160 \pm 0.00025$. The quasar's spectrum was observed on 2003 April 25 and classified as 'excellent' by the SDSS data base.

2.1 Emission line measurements – modelling of the spectrum

In order to study the weak emission line properties of our WLQ, we modelled the spectrum by fitting a power law to the underlying continuum, accounting for blended iron emission (the iron template of Vestergaard & Wilkes 2001 was used) and fitting single Gaussians to the emission and absorption lines. Atmospheric emission lines that still remained after the automatic pipeline reduction were first removed, and the spectrum was corrected for Galactic reddening using the Cardelli, Clayton & Mathis (1989) extinction curve, adopting a colour excess of $E(B-V) = 0.06$ determined from the Galactic neutral hydrogen column from Dickey & Lockman (1990) and Stark et al. (1992), and assuming a fixed conversion of $N(\mathrm{H\,I})/E(B-V) = 5.0 \times 10^{21}\,\mathrm{cm^{-2}\,mag^{-1}}$ (Burstein & Heiles 1978).

The underlying power-law continuum was fitted to regions of spectrum uncontaminated by emission lines and away from blended iron emission. The continuum windows used are shown in Table 1 (model 'Cont') and taken from Forster et al. (2001). Blended iron emission was modelled using the UV iron template of Vestergaard & Wilkes (2001) to spectral windows defined in Forster et al. (2001) (Table 1 model 'Fe1'). We also experimented with slightly modified iron windows which excluded spectral regions of C II] λ2327 and O II λ2441 emission and/or C IV and Mg II narrow absorption line (NAL) absorption (models 'Fe2' and 'Fe3' in Table 1). We present the results of our continuum and iron modelling in Table 2.

In model no. 1 (Cont-Fe1-best in Table 2), we followed the procedure described in Vestergaard & Wilkes (2001), where first the underlying power-law continuum was fitted and subtracted from the spectrum, followed by the modelling of iron emission. The Vestergaard & Wilkes (2001) iron template spectrum was broadened by convolving with Gaussian functions of widths between 900 and 9000 km s^{-1} and separated by steps of 250 km s^{-1}, while conserving the total flux in each template. We chose the broadening value for which χ^2 was lowest. Finally, we subtracted the best iron fit from the spectrum and again fitted the continuum. This procedure was repeated two more times. Final parameters are presented in Table 2.

Table 1. Continuum and iron fitting windows.

Model name	Fitting windows rest-frame wavelength range in Å
Cont[1]	1455–1470, 1690–1700, 2160–2180, 2225–2250, 3010–3040, 3240–3270
Fe1[2]	2020–2120, 2250–2340, 2440–2650, 2900–3000
Fe2[3]	2020–2120, 2250–2300, 2500–2650, 2850–3000
Fe3[4]	1490–1502, 1705–1730, 1760–1800, 2250–2320 2470–2625, 2675–2715, 2735–2755, 2855–3010
ContFe4[5]	1455–1470, 1685–1700, 2020–2120, 2190–2210 2250–2300, 2450–2650, 2850–3070
ContFe5[6]	1440–1470, 1700–1820, 1950–2400, 2450–2700 2850–3100
ContFe6[7]	1455–1470, 1690–1700, 2020–2120, 2160–2180 2225–2650, 2900–3000, 3010–3040, 3240–3270 3350–3400

Column (1) – name of model; Column (2) – wavelength range of spectral windows in which the model was fitted.
[1] – continuum fitted as a power law in Forster et al. (2001) continuum windows;
[2] – iron template fitted in Forster et al. (2001) iron spectral windows, excluding wavelength range 2340–2440 Å (atmosphere artefact + feature at 2350 Å);
[3] – iron template fitted in Forster et al. (2001) iron windows, with regions around C II] λ2327 and O II λ2441 excluded, and 2850–2900 Å window (at red side of Mg II) added for a more consistent fit;
[4] – iron template fitted in spectral windows defined by Vestergaard & Wilkes (2001), with regions of C II] emission and narrow absorption at C IV (1427–1505 Å) and Mg II (2715–2735 Å) excluded;
[5] – power-law continuum and iron emission fitted simultaneously in the 'Cont' and 'Fe1' windows (some windows are narrower or slightly shifted to better match the model with the spectrum);
[6] – power-law continuum and iron emission fitted simultaneously in optimum windows chosen by us and created by comparison of the Richards et al. (2003) composites and Vestergaard & Wilkes (2001) iron template;
[7] – power-law continuum and iron emission fitted simultaneously in the 'Cont' model windows complemented with a 3350–3400 Å window and iron windows from Forster et al. (2001) .

In models no. 2–4 (Cont-Fe1,2,3), a similar procedure was used for the continuum fitting; however, broadening of the iron template and the scaling factor of the amplitude was estimated automatically. We experimented with standard and slightly modified iron windows (models Fe1, Fe2, Fe3 from Table 1).

In models no. 5–7 (i.e. ContFe4,5,6), power-law continuum and iron template were fitted simultaneously (as a sum) to spectral windows including standard and slightly modified continuum and iron windows from Forster et al. (2001) (models 'ContFe4', 'ContFe5' and 'ContFe6' in Table 1).

The best continuum and iron emission fit is represented by model no. 1 (Cont-Fe1-best). It has the lowest reduced χ^2 value and visually gives the best fit to iron emission in the vicinity of the Mg II line, which then leads to the best Mg II emission line fit (as shown by the lowest χ^2 and weakest residuals). In Fig. 1, we plot this continuum and iron emission fit over the rest frame, Galaxy dereddened spectrum of SDSS J094533.99+100950.1. The fit is also included in Fig. 2 and the emission line and central engine properties derived further in the text are made using this model.

The best-fitting continuum has a power-law index, $\alpha_\lambda (f_\lambda \propto \nu^{\alpha_\lambda})$ equal to -1.232 ± 0.017, which is equivalent to $\alpha_\nu = -0.77 (f_\nu \propto \nu^{\alpha_\nu})$. Therefore, the SDSS J094533.99+100950.1 continuum is, in this respect, almost identical to the no. 3 quasar composite

Table 2. Properties of fitted continuum and iron emission template for different fitting windows.

No.		Continuum		Fe II template			χ^2/ndf.	Fitting windows
		α_λ	$F_{3000\,\text{Å}}$ (erg s^{-1} cm^{-2} Å^{-1})	FWHM (km s^{-1})	scalefactor	REW (Å)		
1.	**Cont-Fe1-best**							
	Cont:	-1.232 ± 0.017	$(5.24 \pm 0.69) \times 10^{-16}$	–	–	–	1.51	Cont
	Fe:	–	–	1650 ± 130	0.01176 ± 0.00027	82	1.30	Fe1
2.	Cont-Fe1							
	Cont:	-1.233 ± 0.017	$(5.24 \pm 0.69) \times 10^{-16}$	–	–	–	1.56	Cont
	Fe:	–	–	2150 ± 380	0.01139 ± 0.00027	79	1.30	Fe1
3.	Cont-Fe2							
	Cont:	-1.233 ± 0.017	$(5.24 \pm 0.69) \times 10^{-16}$	–	–	–	1.58	Cont
	Fe:	–	–	2680 ± 420	0.01208 ± 0.00027	84	1.30	Fe2
4.	Cont-Fe3							
	Cont:	-1.240 ± 0.017	$(5.24 \pm 0.69) \times 10^{-16}$	–	–	–	1.58	Cont
	Fe:	–	–	3440 ± 550	0.01070 ± 0.00027	75	1.57	Fe3
5.	ContFe4							
	Cont+Fe:	-1.194 ± 0.011	$(5.40 \pm 0.43) \times 10^{-16}$	1140 ± 190	0.00849 ± 0.00043	58	1.55	ContFe4
6.	ContFe5							
	Cont+Fe:	-1.243 ± 0.010	$(5.22 \pm 0.40) \times 10^{-16}$	2500 ± 300	0.01195 ± 0.00053	85	1.71	ContFe5
7.	ContFe6							
	Cont+Fe:	-1.215 ± 0.012	$(5.35 \pm 0.43) \times 10^{-16}$	1179 ± 190	0.01083 ± 0.00043	74	1.69	ContFe6

Column (1) – model number; Column (2) – model name: fits no. 1–4 have continuum modelled as a power law in spectral windows defined by model 'Cont' in Table 1, independently from the iron emission fitted in iron spectral windows defined by models Fe1,2,3 in Table 1; fits no. 5–7 have continuum and iron emission fit simultaneously to windows defined by models ContFe4,5,6 in Table 1.
Column (3) lists the power-law index, α_λ (where $f_\lambda \propto \lambda^{\alpha_\lambda}$). Column (4) shows the amplitude of the continuum measured at 3000 Å. Columns (5)–(7) list rest-frame FWHM of the Fe II template, scaling factor and Fe II rest-frame equivalent width (REW), respectively. The reduced χ^2 of the fitting procedure is shown in Column (8). Column (9) lists the fitting windows used by us and defined in Table 1.

from Richards et al. (2003). However, we also compared quantitatively the underlying continua of SDSS J094533.99+100950.1 and Richards et al. (2003) composites no. 1–4 by fitting the latter with a power law (to the same spectral windows as for our WLQ – the 'Cont' model from Table 1) and allowing for internal reddening. We checked both Gaskell et al. (2004) and Small Magellanic Cloud (SMC) bar (Sofia et al. 2006) extinction curves. We modified the composites and allowed for either reddening or dereddening. The lowest χ^2 was obtained for composite 4 dereddened by $E(B-V) = 0.75$ for Gaskell et al. (2004) extinction, which is relatively high due to its weak dependence on wavelength, which thus requires large reddening to produce any significant change in spectral shape. For the case of SMC-bar extinction curve a lower value is needed, $E(B-V) = 0.02$. For composite 3 of Richards et al. (2003), no reddening/dereddening was required an acceptable fit. For the other two composites, reddening was required but the fit was always worse than for pure, unreddened composite 3. Since the exact wavelength dependence of the intrinsic reddening in quasars is still under debate, we decided to use composite 3 for comparison. In Fig. 1, we show the Richards et al. (2003) composite no. 3. plotted over the rest-frame SDSS J094533.99+100950.1 spectrum, corrected for Galactic extinction.

Despite the almost identical continua, the two spectra are widely different with respect to the emission line properties. The Mg II emission line is clearly present but the narrow component in the line profile is absent. The contribution of the Fe II and Fe III is almost typical, while the Si III]+C III] and C IV emission is extremely weak compared with a typical quasar. There are also two deep but narrow absorption components (clearly resolved into doublets in the unbinned data plot), blueshifted by $\sim$8300 km s^{-1} with respect to the C IV and Mg II emission line position expected from WLQ's adopted redshift.

The emission and absorption lines were fitted using Gaussians and the fits were performed for all continuum and iron models defined in Table 2. The different models had no significant effect on the absorption line fits (resulting in less than 11 per cent difference in equivalent widths) and so in Table 3 we give the values for one model only Cont-Fe1-best.

The Mg II emission line was more influenced by the choice of continuum and iron models, and the equivalent width varied from fit to fit by a few per cent, with a 15 per cent difference between the Cont-Fe1-best and the extreme value (see Table 4). The measured kinematic width depended on the spectral decomposition, and varied from 5390 up to 6290 km s^{-1}, depending on the model used. However, in all studied cases the line was relatively strong and broad. Therefore, we consider that the properties of the Mg II line are determined reliably which is important from the point of view of black hole mass determination. The C IV line is consistently faint in all models, although some fits indicate the presence of a very weak line while others give values consistent with zero intensity.

For comparison, in Table 5 we give the typical emission line parameters measured for QSOs. Single component fits and two (narrow and broad) component fits are given whenever possible. We see that the Mg II line intensity is a factor of $\sim$2 lower than the mean Mg II line intensity of sources found in the Large Bright Quasar Survey (LBQS; Forster et al. 2001) or observed with the Faint Object Spectrograph (FOS) on the *Hubble Space Telescope* (Kuraszkiewicz et al. 2002) as well as the value found for the single component Mg II fits to the Richards et al. (2003) steep composite. However, C IV line (as well as C III]) is over 20 times fainter. The weakness of C IV – typically one of the strongest quasar lines – qualifies the object as a WLQ. However, the presence of Mg II allows for an estimate of the global physical parameters of our source.

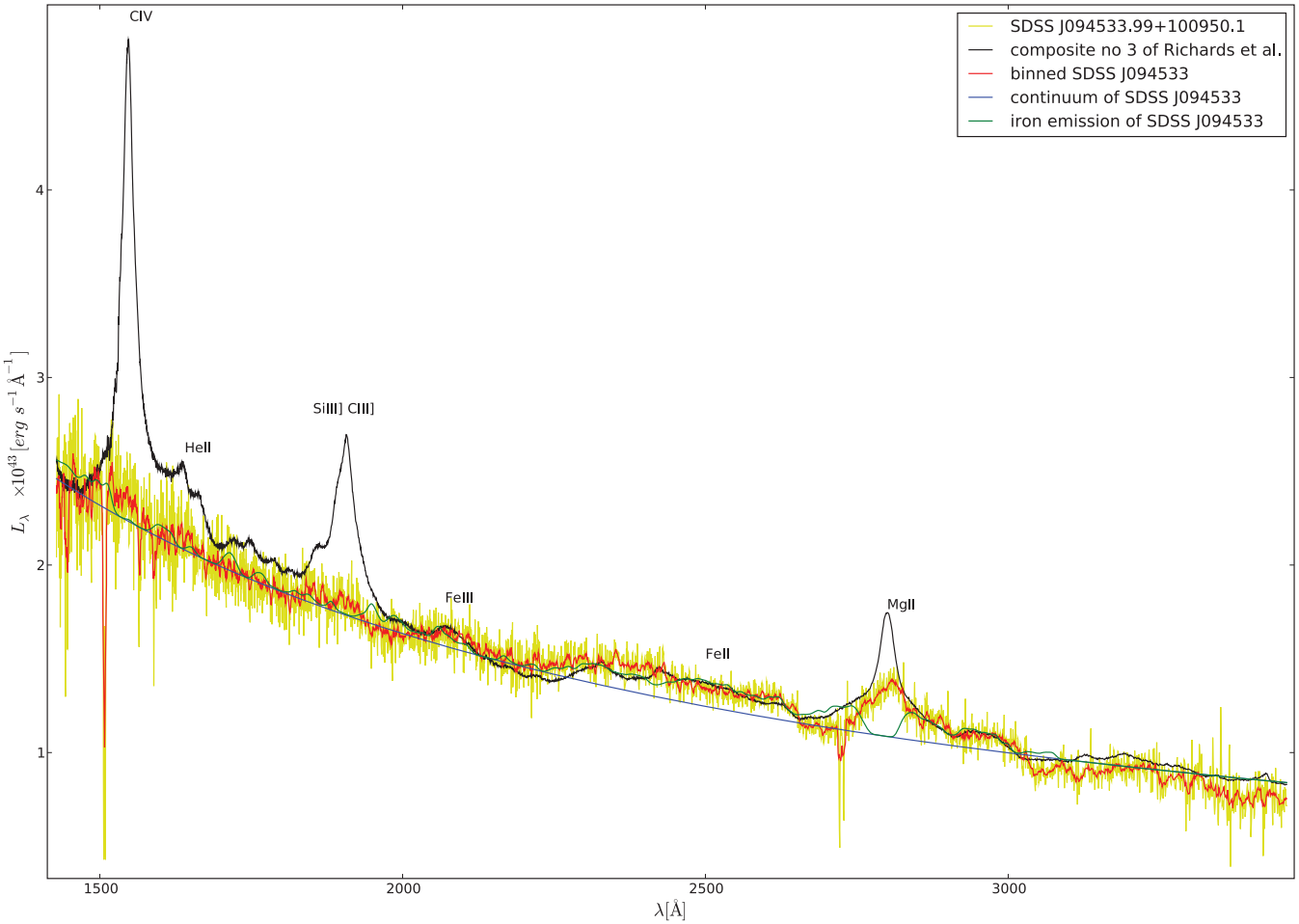

Figure 1. The rest-frame spectrum of SDSS J094533.99+100950.1 corrected for Galactic reddening (yellow line), the binned spectrum of the quasar (red line), its fitted, underlying continuum (blue line) and iron emission (green line). For comparison, in black, the Richards et al. (2003) composite spectrum (no. 3) is shown, greyshifted to match the SDSS J094533.99+100950.1 spectrum.

We also tested the possibility that the redshift determination based on the Mg II line is inaccurate and we allowed the line centroid and the position of the iron line complexes to shift arbitrarily. This did not improve the fit significantly although a possibility of such a shift by a few hundred km s^{-1} cannot be rejected.

Since WLQs have been occasionally suggested to be a BAL (McDowell et al. 1995), we also calculated the BI index (Weymann et al. 1991) in the vicinity of the Mg II line. We obtained a value consistent with zero. Also the AI index (Hall et al. 2002) for this quasar is zero if we take the unbinned spectrum where NAL doublets are clearly resolved – Fig. 2. There is also no sign of a C IV BAL, where the observed spectrum allows detection of such a component blueshifted up to ∼20 000 km s^{-1}. We conclude that SDSS J094533.99+100950.1 is not a BAL or a mini-BAL object.

2.2 Spectral energy distribution

We compiled the broad-band spectral energy distribution (SED) of SDSS J094533.99+100950.1 using the data archives and software of the Virtual Observatory (VO)[1] and the *Galaxy Evolution Explorer* (*GALEX*)[2] data base. This included optical *u*, *g*, *r*, *i* and *z* photometry from SDSS, and near-infrared (near-IR) *J*, *H* and K_s photometry from the Two Micron All Sky Survey (2MASS) and near-UV (NUV) and far-UV (FUV) photometry from *GALEX* (Edge, private communication).

No other spectra or photometric data points were found in the VO within the matching radius of 5 arcsec. All available images of the quasar and its vicinity were downloaded. The quasar is visible in the SDSS and 2MASS images, and also on the Palomar Observatory Sky Survey plates in the optical and near-IR. No X-ray data (*XMM–Newton*, *RXTE*, *INTEGRAL*) were found. We searched for X-ray spectra in the *ROSAT* catalogues, but found no sources with a flux significantly higher than the X-ray background (Sołtan, private communication). The radio properties of our quasar and its neighbourhood were checked in the Parkes-MIT-NRAO (4850 MHz survey), and in the Faint Images of the Radio Sky at Twenty-centimeters (Very Large Array FIRST, 1.4 GHz). In both cases, the radio background was found and the spatial resolution was too low to observe the quasar. The same results were obtained for *IRAS* and *Extreme Ultraviolet Explorer* catalogues – the signal did not differ significantly from the background.

[1]http://www.euro-vo.org/

[2]http://galex.stsci.edu/

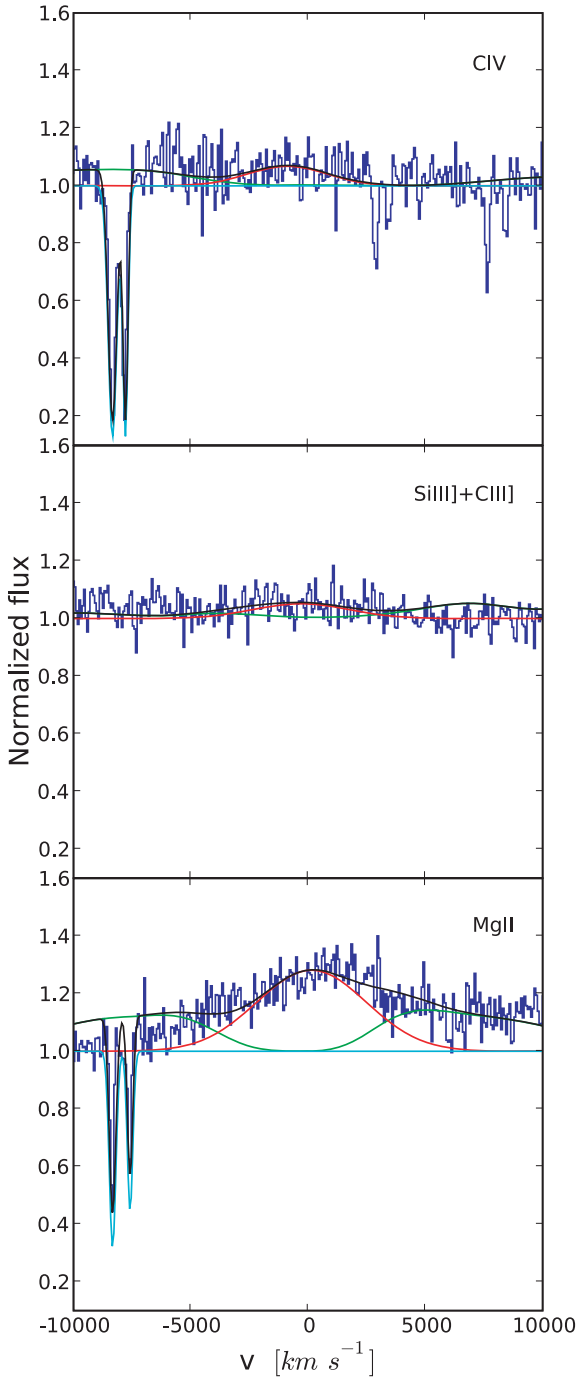

Figure 2. The regions of the C IV, Si III]+C III] and Mg II lines in the spectrum of SDSS J094533.99+100950.1 (blue). Green line shows the broadened [FWHM(Fe II) = 1650 km s^{-1}] iron emission template, red and cyan show fitted emission and absorption lines, respectively, while the black line is sum of all components. Zero velocity was at the theoretical wavelength of each line at a given redshift. The plotted flux was normalized by the continuum.

The SED of SDSS J094533.99+100950.1 is shown in Fig. 3. It does not differ significantly from typical quasar SEDs (e.g. Elvis et al. 1994; Richards et al. 2006), consistent with the conclusion reached by Diamond-Stanic et al. (2009) for other WLQs. The deviation from the Elvis et al. (1994) median SED in the FUV (at NUV and FUV *GALEX* data points) is due to the simple interpolation between the UV and soft X-rays in the Elvis et al. (1994) SED, which does not constrain the true QSO SED at $\lambda < 1000$ Å. However, lower flux in the FUV remains a possibility in our WLQ, which may lead to low C IV emission due to lower ionizing flux.

3 GLOBAL PARAMETERS OF SDSS J094533.99+100950.1

Our WLQ has a monochromatic luminosity at 3000 Å of $\lambda L_\lambda(3000\,\text{Å}) = 2.95 \times 10^{46}\,\text{erg s}^{-1}$, (assuming $H_0 = 71\,\text{km s}^{-1}\,\text{Mpc}^{-1}$, $\Omega_\Lambda = 0.73$ and $\Omega_\text{m} = 0.27$ – Spergel et al. 2007), which is high but not extremely high for a quasar. Using a bolometric correction $\text{BC}_{3000} = 5.15$ determined at 3000 Å (Shen et al. 2008 and Labita et al. 2009, based on Richards et al. 2006), we obtain a bolometric luminosity of $1.52 \times 10^{47}\,\text{erg s}^{-1}$.

We use the following equations from Kong et al. (2006) to determine the central black hole mass:

$$M_\text{BH} = 3.4 \times 10^6 \left(\frac{\lambda L_{3000\,\text{Å}}}{10^{44}\,\text{erg s}^{-1}}\right)^{0.58\pm0.10} \left(\frac{\text{FWHM}_\text{Mg II}}{1000\,\text{km s}^{-1}}\right)^2 \text{M}_\odot \quad (1)$$

$$M_\text{BH} = 2.9 \times 10^6 \left(\frac{L_\text{Mg II}}{10^{42}\,\text{erg s}^{-1}}\right)^{0.57\pm0.12} \left(\frac{\text{FWHM}_\text{Mg II}}{1000\,\text{km s}^{-1}}\right)^2 \text{M}_\odot, \quad (2)$$

where $\lambda L_{3000\,\text{Å}}$ and $L_\text{Mg II}$ are the monochromatic continuum luminosity at 3000 Å and the Mg II line intensity, respectively. Using the Mg II width from the best fit (Cont-Fe1-best in Table 4), we obtain a black hole mass of $2.7 \times 10^9\,\text{M}_\odot$ from equation (1). This is a typical value for a distant quasar (e.g. Kelly et al. 2008; Vestergaard et al. 2008). Using equation (2), we obtain a slightly lower value of the black hole mass, of $1.5 \times 10^9\,\text{M}_\odot$. Similar values of M_BH are obtained when using formulae from McLure & Dunlop (2004).

The first value of the black hole mass implies the Eddington ratio of 0.45. This value is very conservative from the point of view of possible super-Eddington accretion, which is possibly present in some AGN (Collin & Kawaguchi 2004; Jin et al. 2009). It is consistent with several other determinations of this ratio in quasars. Quasars in the redshift range between 1 and 2 in the study of Sulentic et al. (2006) have Eddington ratios between ∼0.2 and ∼1, the value 0.25 is the mean favoured by statistical studies of Shankar et al. (2008). Labita et al. (2009) found a value of 0.45 as a statistical upper limit of accretion rate in their sample of quasars. The second value based on black hole mass from equation (2) gives a somewhat higher ratio of 0.79, which is less reliable because of the weakness of the Mg II emission line. We also computed the mean and standard deviation of the Eddington ratio for all models in Table 2 and obtained the following means: 0.429 ± 0.037 using equation (1) and 0.752 ± 0.077 for equation (2). In the newest studies of the relation between Mg II line parameters and black hole mass, Wang et al. (2009) do not use Mg II equivalent width but rather the Mg II full width at half-maximum (FWHM) and continuum luminosity at 3000 Å. Using the relation from Wang et al. (2009), the mean black hole mass of SDSS J094533.99+100950.1 is $(3.09 \pm 0.23) \times 10^9\,\text{M}_\odot$ and the mean Eddington ratio is 0.396 ± 0.026.

Additionally, since the Mg II emission line intensity is lower than in typical quasars, the second method is probably less reliable than the first, based on the continuum, and so the Eddington ratio of 0.45 is more likely.

Table 3. Rest-frame absorption lines properties of SDSS J094533.99+100950.1

Line	λ_{em} (Å)	λ_0 (Å)	REW (Å)	FWHM (km s^{-1})	Shift (km s^{-1})	z_{abs}
fit: Cont-Fe1-best						
Mg II	2796.357	2721.30 ± 0.51	$-3.79^{+0.34}_{-0.31}$	343 ± 82	-8268 ± 57	1.59016
	2803.536	2728.26 ± 0.58		290 ± 110	-8272 ± 64	1.59013
C IV	1548.189	1506.39 ± 0.22	$-3.35^{+0.42}_{-0.47}$	455 ± 63	-8318 ± 44	1.58975
	1550.775	1509.24 ± 0.24		269 ± 69	-8251 ± 49	1.59031

Column (1) – name of absorption line, Column (2) – the wavelength of the line seen in laboratory. The absorption lines were fitted with Gaussians to a dereddened, rest frame, Fe II subtracted quasar spectrum. Column (3) – wavelength of the minimum intensity of the line in the fit. Column (4) – REW of the doublet (computed as a sum of two Gaussians). Column (5) – FWHM of the absorption line. Column (6) lists the line blueshift in km s^{-1} . We present measurements for the Cont-Fe1-best model from Table 2 only, as other models gave similar results.

Table 4. Rest-frame emission lines properties of SDSS J094533.99+100950.1.

Line	λ_0 (Å)	REW (Å)	FWHM (km s^{-1})	z_{em}
fit: Cont-Fe1-best				
Mg II λ2800	2800.29 ± 0.79	$15.3^{+1.1}_{-1.1}$	5490 ± 220	1.66187
C III] λ1909 + Si III] λ1892	1906.7 ± 2.3	$1.68^{+0.61}_{-0.52}$	4800 ± 4800	1.65845
C IV λ1549	1544.9 ± 2.3	$1.49^{+0.82}_{-0.64}$	4000 ± 1100	1.65451
fit: Cont-Fe1				
Mg II λ2800	2800.60 ± 0.81	$15.5^{+1.1}_{-1.1}$	5690 ± 230	1.66217
C III] λ1909 + Si III] λ1892	1905.6 ± 2.4	$1.69^{+0.63}_{-0.53}$	5000 ± 5000	1.65680
C IV λ1549	1545.6 ± 2.2	$1.41^{+0.79}_{-0.62}$	3800 ± 1100	1.65572
fit: Cont-Fe2				
Mg II λ2800	2800.85 ± 0.83	$15.2^{+1.1}_{-1.1}$	5750 ± 240	1.66240
C III] λ1909 + Si III] λ1892	1904.6 ± 2.5	$1.69^{+0.64}_{-0.54}$	5100 ± 5100	1.65539
C IV λ1549	1545.9 ± 2.3	$1.36^{+0.78}_{-0.60}$	3800 ± 1100	1.65632
fit: Cont-Fe3				
Mg II λ2800	2801.64 ± 0.92	$15.9^{+1.2}_{-1.2}$	6290 ± 270	1.66316
C III] λ1909 + Si III] λ1892	1903.9 ± 2.7	$1.64^{+0.66}_{-0.55}$	5200 ± 5200	1.65455
C IV λ1549	1545.7 ± 2.5	$1.18^{+0.77}_{-0.58}$	3600 ± 1200	1.65597
fit: ContFe4				
Mg II λ2800	2799.28 ± 0.91	$14.0^{+1.2}_{-1.1}$	5670 ± 250	1.66091
C III] λ1909 + Si III] λ1892	1905.6 ± 2.5	$1.37^{+0.59}_{-0.48}$	4400 ± 4400	1.65680
C IV λ1549	1543.7 ± 2.6	$1.59^{+0.91}_{-0.71}$	4300 ± 1300	1.65252
fit: ContFe5				
Mg II λ2800	2804.77 ± 0.76	$16.0^{+1.1}_{-1.1}$	5600 ± 220	1.66614
C III] λ1909 + Si III] λ1892	1902.5 ± 2.5	$1.91^{+0.68}_{-0.58}$	5400 ± 5400	1.65252
C IV λ1549	1547.4 ± 2.4	$1.11^{+0.73}_{-0.55}$	3400 ± 1100	1.65888
fit: ContFe6				
Mg II λ2800	2798.84 ± 0.87	$14.1^{+1.2}_{-1.1}$	5390 ± 240	1.66050
C III] λ1909 + Si III] λ1892	1906.0 ± 2.4	$1.33^{+0.58}_{-0.47}$	4300 ± 4300	1.65738
C IV λ1549	1543.7 ± 2.6	$1.45^{+0.89}_{-0.68}$	4200 ± 1300	1.65244

Column (1) – name of emission line, Column (2) – wavelength of the maximum intensity of the line in the fit (emission lines were fitted with a Gaussian to a dereddened, rest frame, Fe II subtracted quasar spectrum), Column (3) – REW of the line, Column (4) – FWHM of the emission line, Column (5) – redshift.
The fitting window for Mg II is 2750–2840 Å, for C IV 1530–1580 Å and for C III] + Si III] 1880–1940 Å.

4 DISCUSSION

The WLQ SDSS J094533.99+100950.1 is an exceptional object with almost non-existent C IV emission, normal Fe II emission and visible, although somewhat fainter and atypical, Mg II emission line. The presence of iron emission with standard intensity argues against any relativistic enhancement of the continuum in this source. The quasar continuum is normal, similar to the steep composite no. 3 of Richards et al. (2003).

The lack of strong emission lines (except for Mg II) is likely to be intrinsic, consistent with the conclusion reached by Diamond-Stanic et al. (2009) for other WLQs. A remarkable property of the SDSS

Table 5. Emission line properties in other quasar samples.

Line	REW(composite) (Å)	REW(FOS) (Å)	FWHM (FOS) (km s^{-1})	REW (LBQS) (Å)	FWHM (LBQS) (km s^{-1})
Mg II					
single	30.14	136 ± 92[1]	3840 ± 1850	39 ± 22	5160 ± 120
broad		33 ± 8	8230 ± 1850	37 ± 22	8660 ± 300
narrow		29 ± 9	3260 ± 760	28 ± 13	3510 ± 110
C III]	21.45	21 ± 5	4890 ± 780	28 ± 15	7820 ± 170
C IV					
single	26.86	21 ± 16[1]	4430 ± 3070	38 ± 20	7720 ± 150
broad		63 ± 7	11090 ± 1070	45 ± 23	10960 ± 360
narrow		30 ± 4	2900 ± 290	17.8 ± 9.3	2860 ± 110

Emission line parameters of SDSS J094533.9+100950 are compared with: in Column (2) the Richards et al. (2003) composite no. 3 (Fig. 1) built on the basis of 770 quasar spectra, in Columns (3), (4) the 158 AGN observed with FOS on the *Hubble Space Telescope* (heterogeneous sample of mixed type AGN; Kuraszkiewicz et al. 2002) and in Columns (5), (6) the 993 quasars from the LBQS (Forster et al. 2001). In Column (1), 'single' means that the line was fitted by a single Gaussian, while 'broad' and 'narrow' refer to the broad and narrow components of the line.
[1] – The single Gaussian fits to Mg II and C IV emission lines in FOS were based only on a few, low-quality spectra and thus may not be representative.

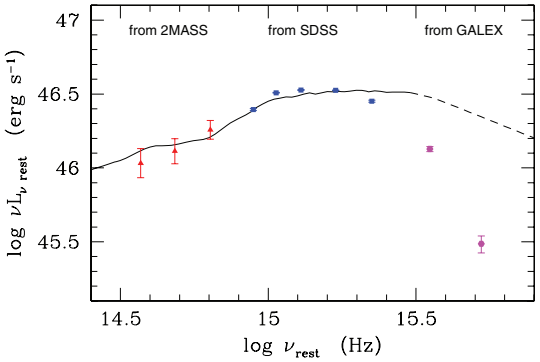

Figure 3. The broad-band SED of SDSS J094533.99+100950.1. The photometric IR data point (triangles) come from 2MASS (J, H, K_s colours). Optical photometry (squares) is from SDSS (u,g,r,i,z filters). The NUV and FUV points (hexagons) are from *GALEX*. The spatial coordinates of the source differ between SDSS and 2MASS by ∼0.39 arcsec and between SDSS and *GALEX* by ∼0.48 arcsec. We assume the data from SDSS, 2MASS and *GALEX* come from the same object. Galactic dereddening was done using the values $E(B-V) = 0.060$, $R_V = 3.2$ and formulae of Cardelli et al. (1989). Neither intrinsic dereddening of the quasar nor subtraction of Fe II were done. For comparison, the line shows the SED from Elvis et al. (1994) marking with dashed line the frequency range of interpolation between the FUV and soft X-ray band.

J094533.99+100950.1 spectrum is the presence of low ionization lines (LILs) such as Mg II, which are thought to form close to the accretion disc surface (see e.g. Collin-Souffrin et al. 1988) and the absence of high ionization lines (HILs) such as C IV. The narrow component of Mg II, which is thought to form at larger distances from the nucleus, is also absent from the spectrum.

McDowell et al. (1995) listed 10 possible explanations for the weakness of emission lines in their WLQ, PG 1407+265, but rejected most of them on the basis of overall quasar properties. Among those remaining are: high extinction or BAL effects, which are inconsistent with SDSS J094533.99+100950.1 properties, and abnormal ionizing continuum, which remains a possibility. In particular, the option of high (super-Eddington) accretion rate may seem attractive since the determination of the Eddington ratio for our object allows (but does not require) for such a possibility (see Section 3). However, the expected trends found by principal components analysis (PCA) performed on the optical/UV emission line properties of Palomar-Green QSO (Shang et al. 2003, see fig. 10) show that, with increasing Eddington ratio, the UV Fe II emission (measured around Mg II) decreases,[3] Si III]+C III] emission increases and the widths of Mg II and Si III]+C III] lines decrease. The opposite is seen in our object. Additionally, the Si IV line should become stronger, but this is not seen in the WLQs of Shemmer et al. (2009). Since the emission line properties of WLQs do not follow the trends for high L/L_{Edd} objects predicted by PCA analysis, something different than high L/L_{Edd} is causing the atypical emission line behaviour.

The only explanation, which in our opinion is currently consistent with the intriguing emission line properties of our WLQ, is that the quasar activity in this source has just begun.

The formation of an accretion disc in an AGN is a long time phenomenon, occurring in millions of years (the viscous time-scale in the outer disc; Siemiginowska, Czerny & Kostyunin 1996). However, when the disc finally approaches a black hole, i.e. when the inner radius moves from ∼ 10 to 20 R_{Schw} to inner stable circular orbit, the disc's luminosity rapidly increases on a hundred year time-scale and X-ray emission starts (Czerny 2006).

The immediate stage after is the irradiation of the outer disc which happens in the light traveltime across the region (years). At this stage, the accretion disc continuum appears already to be typical for an AGN. However, neither the broad-line region (BLR) nor the narrow-line region (NLR) region exist.

If our explanation is correct, our WLQ should have no narrow [O III]λ5007 emission but its LIL Hβ line should have already formed (as has the Mg II line). For our $z = 1.6$ object, these lines lie outside the observed wavelength range of the optical telescopes used by SDSS, but could, in principle, be observed using an IR facility. In another WLQ, PG 1407+265 (McDowell et al. 1995), the Hβ line is weak, contrary to our expectations. However, significant influence of the atmosphere above 9000 Å leading to low spectrum quality at those wavelengths may partially hide the line (see fig. 1 of McDowell et al. 1995). The puzzling properties of the

[3] not increases, as is the case for optical Fe II measured around Hβ.

X-ray emission of PG 1407+265 may be consistent with the young age of the source as the emission significantly varies in time, and is only occasionally dominated by a jet (Gallo 2006) indicating that a stable jet has not yet been launched.

A relatively young age was also suggested for the class of narrow-line Seyfert 1 (NLS1) galaxies, in the context of cosmological evolution (Mathur 2000) but their BLR is well developed. WLQs thus possibly represent an even earlier stage but not necessarily in the sense of a global evolution since the argument of their young age is based on BLR formation stage. If the observed activity is the first active stage of the nucleus, then indeed the WLQ stage should be seen first, later replaced by the NLS1 stage (with efficient growth of the central black hole), followed by the broad emission line stage (quasar or Seyfert 1). However, it is also possible that the observed active stage represents the source's reactivation. The amount of intrinsic (nuclear) dust along the line of sight does not seem to be large and the past activity may be the natural explanation for such a clean environment for an otherwise young object. The large mass of the black hole, particularly in PG 1407+265 ($\log M_{\rm BH} = 9.8$ based on C IV FWHM and the formula of Vestergaard & Peterson 2006) might rather indicate a relatively late evolutionary stage, favouring the reactivation scenario. A few stages of quasar life are also predicted by Hopkins & Hernquist (2009). They postulate that the life of quasars consists of a merger and a few episodes of high accretion rate. The activity is likely to cease through a 'naked' AGN stage (Williams, Baker & Perry 1999; Hawkins 2004) since when the accretion rate drops, the optical disc recedes outward and the component of the BLR linked to the disc wind disappears (e.g. Czerny, Różańska & Kuraszkiewicz 2004; Elitzur & Ho 2009).

An intermittent character for the quasar activity is also more consistent with the statistics of WLQ. The sources are rare but not as rare as we might expect (based on the following discussion). The irradiation causes the formation of a wind in the upper disc atmosphere, and this material slowly rises up in the vertical direction. This wind is customarily now considered as the source of the material from BLR clouds (Murray et al. 1995; Proga, Stone & Kallman 2000; Chelouche & Netzer 2003; Everett 2005). The initial rise is not highly supersonic. Assuming velocities $\sim$100 km s^{-1} (e.g. Proga 2003; Everett 2005), we can estimate how much time the material takes to depart significantly from the disc's surface layers. Assuming a disc radius of 1 pc, a rise by 10 per cent of the radial distance takes 1000 yr, and at that stage the LILs forming close to the disc, like Mg II and Hβ appear. The rise to the height comparable to the radial distance takes a factor of 10 times longer, and only after that time the highly ionized lines such as C IV appear in the spectrum. The narrow emission line components take longer to form and are likely to be absent at the initial stages. A similar argument was used for the explanation of the relative faintness of the [O III] line in gigahertz peaked spectrum quasars which are also thought to be relatively young (Vink et al. 2006). Thus, a WLQ phase lasts for about 1000 yr. There are almost 100 quasars classified as WLQ (Diamond-Stanic et al. 2009; Shemmer et al. 2009; Plotkin et al. 2010) in the whole sample of $\sim$100 000 SDSS quasars. However, only a fraction of those, including SDSS J094533.99+100950.1 (this paper), PG 1407+265 (McDowell et al. 1995) and HE 0141-3932 (Reimers et al. 2005), may represent a more advanced stage with partially developed LILs. Therefore, the probability of observing this evolutionary stage can be estimated as 10^{-3}–10^{-4}. This would indicate that the typical duration of a quasar's active phase is only $\sim 10^6$–10^7 yr. On the other hand, the lifetime of the luminous phase of quasars is $\sim 10^7 < t_{\rm QSO} < \sim 10^8$ yr (Haiman & Hui 2001), but in some sources extends over a period $\sim 10^9$ yr (Martini & Weinberg 2001). The two numbers can be reconciled if the total active phase of a quasar consists typically of 100 separate subphases, each of those starting with a WLQ stage of BLR buildup.

The increasing probability of occurrence of WLQ among high-redshift objects (Diamond-Stanic et al. 2009) agrees with our hypothesis if, in the earlier Universe, minor mergers are more frequent and the typical single active subphase lasts shorter.

Thus, the SDSS J094533.99+100950.1 quasar with its remarkable properties may have a Rosetta stone impact on our understanding of quasar activity cycle and the nature of WLQ.

Finally, it is important to note that the definition of a WLQ has not been yet worked out. Some objects with extremely faint/non-existent lines may indeed be BL Lacs. Others, like PHL 1811 (Leighly et al. 2007), considered as a WLQ prototype, may be explained by higher Eddington ratio since the lines are not only fainter but also narrower (Mg II line of 2550 ± 110 km s^{-1} versus 5490 ± 220 km s^{-1} in J094533.99+100950.1). Our hypothesis of young/newly active sources would not apply to those classes of objects.

5 CONCLUSIONS

Quasar SDSS J094533.99+100950.1 is an exceptional example of the WLQ class. The broad-band spectrum is typical for quasars, very similar to the second steepest composite spectrum of Richards et al. (2003). It has a relatively well-developed broad Mg II line and the typical Fe II contribution but its HILs, like C IV, are weak/absent. The BAL phenomenon is not visible in the spectrum, so the lack of C IV line is an intrinsic property of the source. The presence of Mg II and typical Fe II emission excludes a non-thermal, blazar-like origin of the spectrum. The significant width of Mg II line (FWHM of 5500 km s^{-1}) and the Fe II properties argue in turn against an extremely high accretion rate in this object. Objects like these are difficult to find since a typical search for WLQs, based on finding spectra with extremely weak or non-existent emission lines, is likely to miss sources where one of the lines is relatively strong. However, such objects are important to find/study as they are likely to shed light on the mechanism driving all (or at least some) WLQs.

In the present paper, we propose the following hypothesis for the nature of WLQ. AGN are generally classified according to their viewing angle and Eddington ratio. However, those objects evolve and some evolutionary stages may be too short to produce a consistent equilibrium between various emitting components in the nucleus like the BLR, NLR and the accretion disc. It is an interesting possibility that the WLQ class represents such a stage, at the onset of quasar activity. The relatively high occurrence of these sources may additionally suggest that a quasar's active phase has an intermittent character. The whole active phase consists of several subphases, each starting with a slow development of the BLR region which manifests itself as a WLQ phenomenon. Further observational tests of this hypothesis are clearly needed.

ACKNOWLEDGMENTS

We would like to thank an anonymous referee for useful comments that improved our paper. We are grateful to Marianne Vestergaard for providing us with the iron emission template. We would also like to thank Andrzej Sołtan for data search in *ROSAT* catalogues, Alastair Edge for helpful remarks about *GALEX* and 2MASS missions and Belinda Wilkes for advices during improving this paper. This work makes use of EURO-VO software, tools or services. The EURO-VO has been funded by the European Commission through contract

numbers RI031675 (DCA) and 011892 (VO-TECH) under the 6th Framework Programme and contract number 212104 (AIDA) under the 7th Framework Programme. This work was supported in part by N N203 380136 and by the Polish Astroparticle Network 621/E-78/BWSN-0068/2008.

REFERENCES

Adelman-McCarthy J. K. et al., 2007, ApJS, 172, 634
Anderson S. F. et al., 2001, AJ, 122, 503
Burstein D., Heiles C., 1978, ApJ, 225, 40
Cardelli J. A., Clayton G. C., Mathis J. S., 1989, ApJ, 345, 245
Chelouche D., Netzer H., 2003, MNRAS, 344, 223
Collin S., Kawaguchi T., 2004, A&A, 426, 797
Collin-Souffrin S., Dyson J. E., McDowell J. C., Perry J. J., 1988, MNRAS, 232, 539
Collinge M. J. et al., 2005, AJ, 129, 2542
Czerny B., 2006, in Gaskell C. M., McHardy I. M., Peterson B. M., Sergeev S. G., eds, ASP Conf. Ser. Vol. 360, AGN Variability from X-Rays to Radio Waves. Astron. Soc. Pac., San Francisco, p. 265
Czerny B., Różańska A., Kuraszkiewicz J., 2004, A&A, 428, 39
Diamond-Stanic A. M. et al., 2009, ApJ, 699, 782
Dickey J. M., Lockman F. J., 1990, ARA&A, 28, 215
Dobrzycki A., Engels D., Hagen H.-J., 1999, A&A, 349, L29
Elitzur M., Ho L. C., 2009, ApJ, 701, L91
Elvis M. et al., 1994, ApJS, 95, 1
Everett J. E., 2005, ApJ, 631, 689
Fan X. et al., 1999, ApJ, 526, L57
Forster K., Green P. J., Aldcroft T. L., Vestergaard M., Foltz C. B., Hewett P. C., 2001, ApJS, 134, 35
Gallo L. C., 2006, MNRAS, 365, 960
Gaskell C. M., Goosmann R. W., Antonucci R. R. J., Whysong D. H., 2004, ApJ, 616, 147
Haiman Z., Hui L., 2001, ApJ, 547, 27
Hall P. B. et al., 2002, ApJS, 141, 267
Hawkins M. R. S., 2004, A&A, 424, 519
Hopkins Ph. F., Hernquist L., 2009, ApJ, 698, 1550
Jin C. C., Done C., Ward M., Gierliński M., Mullaney J., 2009, MNRAS, 398, 16
Kelly B. C., Bechtold J., Trump J. R., Vestergaard M., Siemiginowska A., 2008, ApJS, 176, 355
Kong M.-Z., Wu X.-B., Wang R., Han J.-L., 2006, Chin. J. Astron. Astrophys., 6, 396
Kuraszkiewicz J. K., Green P. J., Forster K., Aldcroft T. L., Evans I. N., Koratkar A., 2002, ApJS, 143, 257
Labita M., Decarli R., Treves A., Falomo R., 2009, MNRAS, 396, 1537
Leighly K. M., Halpern J. P., Jenskins E. B., Casebeer D., 2007, ApJS, 173, 1
McDowell J. C., Canizares C., Elvis M., Lawrence A., Markoff S., Mathur S., Wilkes B. J., 1995, ApJ, 450, 585
McLure R. J., Dunlop J. S., 2004, MNRAS, 352, 1390
Martini P., Weinberg D. H., 2001, ApJ, 547, 12
Mathur S., 2000, MNRAS, 314, L17
Murray N., Chiang J., Grossman S. A., Voit G. M., 1995, ApJ, 451, 498
Plotkin R. M. et al., 2010, AJ, 139, 390
Proga D., 2003, ApJ, 585, 406
Proga D., Stone J. M., Kallman T. R., 2000, ApJ, 543, 686
Reimers D., Janknecht E., Fechner C., Agafonova I. I., Levshakov S. A., Lopez S., 2005, A&A, 435, 17
Richards G. T. et al., 2002, AJ, 123, 2945
Richards G. T. et al., 2003, AJ, 126, 1131
Richards G. T. et al., 2006, ApJS, 166, 470
Schneider D. P. et al., 2007, AJ, 134, 102
Shang Z., Wills B. J., Robinson E. L., Wills D., Laor A., Xie B., Yuan J., 2003, ApJ, 586, 52
Shankar F., Crocce M., Miralda-Escude J., Fosalba P., Weinberg D. H., 2008, ApJ, submitted (arXiv:0810.4919)
Shemmer O. et al., 2006, ApJ, 644, 86
Shemmer O. et al., 2009, ApJ, 696, 580
Shen Y., Greene J. E., Strauss M. A., Richards G. T., Schneider D. P., 2008, ApJ, 680, 169
Siemiginowska A., Czerny B., Kostyunin V., 1996, ApJ, 458, 491
Sofia U. J., Gordon K. D., Clayton G. C., Misselt K., Wolff M. J., Cox N. L. J., Ehrenfreund P., 2006, ApJ, 636, 753
Spergel D. N. et al., 2007, ApJS, 170, 377
Stark A., Gammie Ch. F., Wilson R. W., Bally J., Linke R. A., Heiles C., Hurwitz M., 1992, ApJS, 79, 77
Sulentic J. W., Repetto P., Stirpe G. M., Marziani P., Dultzin-Hacyan D., Calvani M., 2006, A&A, 456, 929
Vestergaard M., Peterson B. M., 2006, ApJ, 641, 689
Vestergaard M., Wilkes B. J., 2001, ApJS, 134, 1
Vestergaard M., Fan X., Tremonti C. A., Osmer P. S., Richards G. T., 2008, ApJ, 674, L1
Vink J., Snellen I., Mack K.-H., Schilizzi R., 2006, MNRAS, 367, 928
Wang J.-G. et al., 2009, ApJ, 707, 1334
Wayth R. B., O'Dowd M., Webster R. L., 2005, MNRAS, 359, 561
Weymann R. J., Morris S. L., Folts C. B., Hewett P. C., 1991, ApJ, 373, 23
Williams R. J. R., Baker A. C., Perry J. J., 1999, MNRAS, 310, 913

This paper has been typeset from a TEX/LATEX file prepared by the author.